

UNVEILING THE NATURE OF SUBMILLIMETER GALAXY SXDF 850.6

B. HATSUKADE¹, D. IONO², T. YOSHIKAWA³, M. AKIYAMA³, J. S. DUNLOP⁴, R. J. IVISON^{5,4}, A. B. PECK⁶, S. IKARASHI¹,
A. BIGGS⁷, H. EZAWA⁸, H. HANAMI⁹, P. HO¹⁰, D. H. HUGHES¹¹, R. KAWABE², K. KOHNO^{1,12}, S. MATSUSHITA¹⁰,
K. NAKANISHI², N. PADILLA¹³, G. PETITPAS¹⁴, Y. TAMURA², J. WAGG^{11,15,16}, D. J. WILNER¹⁶, G. W. WILSON¹⁷,
T. YAMADA³, AND M. S. YUN¹⁷

Accepted for Publication in the Astrophysical Journal

ABSTRACT

We present an 880 μm Submillimeter Array (SMA) detection of the submillimeter galaxy SXDF 850.6. SXDF 850.6 is a bright source ($S_{880\mu\text{m}} = 8$ mJy) detected in the SCUBA Half Degree Extragalactic Survey (SHADES), and has multiple possible radio counterparts in its deep radio image obtained at the VLA. Our new SMA detection finds that the submm emission coincides with the brightest radio emission that is found $\sim 8''$ north of the coordinates determined from SCUBA. Despite the lack of detectable counterparts in deep UV/optical images, we find a source at the SMA position in near-infrared and longer wavelength images. We perform SED model fits to UV–optical–IR photometry ($u, B, V, R, i', z', J, H, K$, 3.6 μm , 4.5 μm , 5.8 μm , and 8.0 μm) and to submm–radio photometry (850 μm , 880 μm , 1100 μm , and 21 cm) independently, and we find both are well described by starburst templates at a redshift of $z \simeq 2.2 \pm 0.3$. The best-fit parameters from the UV–optical–IR SED fit are a redshift of $z = 1.87_{-0.07}^{+0.15}$, a stellar mass of $M_{\star} = 2.5_{-0.3}^{+2.2} \times 10^{11} M_{\odot}$, an extinction of $A_V = 3.0_{-1.0}^{+0.3}$ mag, and an age of 720_{-210}^{+1880} Myr. The submm–radio SED fit provides a consistent redshift of $z \sim 1.8$ –2.5, an IR luminosity of $L_{\text{IR}} = (7$ –26) $\times 10^{12} L_{\odot}$, and a star formation rate of 1300–4500 $M_{\odot} \text{ yr}^{-1}$. These results suggest that SXDF 850.6 is a mature system already having a massive amount of old stellar population constructed before its submm bright phase and is experiencing a dusty starburst, possibly induced by major mergers.

Subject headings: galaxies: formation, galaxies: starburst, cosmology: observations, galaxies: high redshift, submillimeter

1. INTRODUCTION

¹ Institute of Astronomy, the University of Tokyo, 2-21-1 Osawa, Mitaka, Tokyo 181-0015, Japan

Electronic address: hatsukade@ioa.s.u-tokyo.ac.jp

² Nobeyama Radio Observatory, Minamimaki, Minamisaku, Nagano 384-1805, Japan

³ Astronomical Institute, Tohoku University, Aramaki, Aoba-ku, Sendai, Miyagi 980-8578, Japan

⁴ Scottish Universities Physics Alliance, Institute for Astronomy, School of Physics and Astronomy, University of Edinburgh, Royal Observatory, Edinburgh EH9 3HJ, UK

⁵ UK Astronomy Technology Centre, Science and Technology Research Council, Royal Observatory, Blackford Hill, Edinburgh EH9 3HJ, UK

⁶ Joint ALMA Observatory, Avenida El Golf 40, Piso 18, Las Condes 7550108 Santiago, Chile

⁷ European Southern Observatory, Karl-Schwarzschild-Straße 2, D-85748 Garching, Germany

⁸ National Astronomical Observatory of Japan, 2-21-1 Osawa, Mitaka, Tokyo 181-8588, Japan

⁹ Physics Section, Faculty of Humanities and Social Sciences, Iwate University, Morioka 020-8550, Japan

¹⁰ Academia Sinica Institute of Astronomy and Astrophysics, P.O. Box 23-141, Taipei 10617, Taiwan

¹¹ Instituto Nacional de Astrofísica, Óptica y Electrónica (INAOE), Aptdo. Postal 51 y 216, 72000 Puebla, Pue., Mexico

¹² Research Center for the Early Universe, University of Tokyo, 7-3-1 Hongo, Bunkyo, Tokyo 113-0033, Japan

¹³ Departamento de Astronomía y Astrofísica, Pontificia Universidad Católica de Chile, Vicuña Mackenna 4860, Santiago, Chile

¹⁴ Harvard-Smithsonian Center for Astrophysics, Submillimeter Array, 645 North A'ohoku Place, Hilo, HI 96720, USA

¹⁵ European Southern Observatory, Alonso de Córdova 3107, Vitacura, Casilla 19001, Santiago 19, Chile

¹⁶ Harvard-Smithsonian Center for Astrophysics, 60 Garden Street, Cambridge, MA 02138, USA

¹⁷ University of Massachusetts, Department of Astronomy, Amherst, MA 01003, USA

Millimeter/submillimeter surveys have revolutionized observational cosmology by uncovering a substantial new population of mm/submm-bright dusty starburst galaxies at high redshifts (SMGs) (e.g., Smail, Ivison & Blain 1997; Barger et al. 1998; Hughes et al. 1998; Scott et al. 2002; Coppin et al. 2006; Greve et al. 2004; Laurent et al. 2005; Scott et al. 2008; Perera et al. 2008; Austermann et al. 2009; Tamura et al. 2009, and see also Blain et al. 2002 for a review). The energy source of mm/submm emission is primarily from intense star formation activity, with star formation rates (SFRs) of 100 $M_{\odot} \text{ yr}^{-1}$ to several 1000 $M_{\odot} \text{ yr}^{-1}$, and possibly partially from an active galactic nucleus (AGN) (e.g., Alexander et al. 2005). While spectroscopic observations of radio-identified SMGs find a median redshift of 2.2 (Chapman et al. 2005), several SMGs have now been found up to and beyond $z = 4$ (e.g., Capak et al. 2008; Coppin et al. 2009; Daddi et al. 2009). There is a hypothesis that SMGs are progenitors of present-day massive ellipticals (e.g., Lilly et al. 1999; Smail et al. 2004), however, little is known about their evolution process.

While multi-wavelength analysis is essential in order to understand the nature of SMGs, the coarse angular resolution of single dish telescopes prevents a precise determination of the exact optical/NIR counterparts. One of the most successful ways to pinpoint the location of the submm emission is to obtain high resolution, deep radio imaging (e.g. Ivison et al. 1998, 2000, 2002; Smail et al. 2000; Barger et al. 2000). Although this technique reveals robust radio counterparts of $\sim 50\%$ –80% of submm sources (e.g., Ivison et al. 2005, 2007;

Wagg et al. 2009), sometimes multiple radio counterpart candidates are found for a source.

The most accurate means of achieving high precision astrometry on the submillimeter emission is clearly to observe with high angular resolution at the wavelength of the original detection. In this respect, the Submillimeter Array (SMA; Ho et al. 2004) has proved to be a powerful instrument (Iono et al. 2006a,b; Wang et al. 2007; Younger et al. 2007, 2008; Ivison et al. 2008).

Here we present the results from the SMA observations toward an 8 mJy submm source, SXDF 850.6, detected in the SCUBA Half Degree Extragalactic Survey (SHADES). SHADES has observed a large area of the sky (720 arcmin^2) with high sensitivity ($1\sigma \sim 2 \text{ mJy}$) with the purpose of obtaining a statistically significant unbiased sample of submillimeter sources (Mortier et al. 2005; Coppin et al. 2006). The regions covered by SHADES are divided between two fields, the Lockman Hole and the Subaru/*XMM-Newton* Deep Field (SXDF). SXDF 850.6 is a source in the SXDF with multiple optical, IR, and radio counterparts (Ivison et al. 2007; Clements et al. 2008), but no established submm source identification. The strongest radio emission has no confirmed optical counterpart, but the two secondary radio peaks both have apparent optical associations.

§ 2 outlines the observational and calibration details, and the results are presented in § 3. In § 4, multi-wavelength data are described. The results of SED model fitting using the photometry are presented in § 5. In § 6, we discuss the nature of SXDF 850.6. A summary is presented in § 7. Throughout the paper, magnitudes are in the AB system, and we adopt a cosmology with $H_0 = 70 \text{ km s}^{-1} \text{ Mpc}^{-1}$, $\Omega_M = 0.3$, and $\Omega_\Lambda = 0.7$.

2. OBSERVATIONS AND DATA REDUCTION

SXDF 850.6 was observed on September 21 and October 7, 2004, and on October 9 and 14, 2005, using a compact configuration with 7 – 8 antennas of the SMA. The phase center was positioned at the submm source centroid which is $\alpha(\text{J2000}) = 02^{\text{h}} 17^{\text{m}} 29.80^{\text{s}}$ and $\delta(\text{J2000}) = -05^{\circ} 03' 26''.00$. The unprojected baseline length ranged from 23 m to 139m. The SMA correlator was equipped with 2 GHz total bandwidth in each sideband, yielding a total of 4 GHz bandwidth for continuum observations. A continuum channel was generated by vector averaging all of the channels after calibration. The SIS receivers were tuned to 345 GHz for the USB, yielding 335 GHz for the LSB. Interferometric pointing was checked at the beginning of the track and the pointing offsets were usually within $\sim \pm 5''$ (15% of the primary beam) for all antennas. We used an integration time of 30 seconds.

The raw SMA data was calibrated using the MIR package (Scoville et al. 1993). Passband calibration was done using bright QSOs and planets observed during the track. Antenna based phase calibration was done using J0238+166 (1.02 Jy), J0423-013 (1.67 Jy) and J0132-169 (0.84 Jy). The flux levels of all sources were normalized using the the quasar flux estimates derived from the primary flux standard Uranus. Imaging was carried out in MIRIAD (Sault et al. 1995). Maximum sensitivity was achieved by adopting natural weighting, which gave a final synthesized beam size of $2''.32 \times 2''.19$ (P.A. = 79.1°) and an RMS noise of 1.2 mJy. Because the source

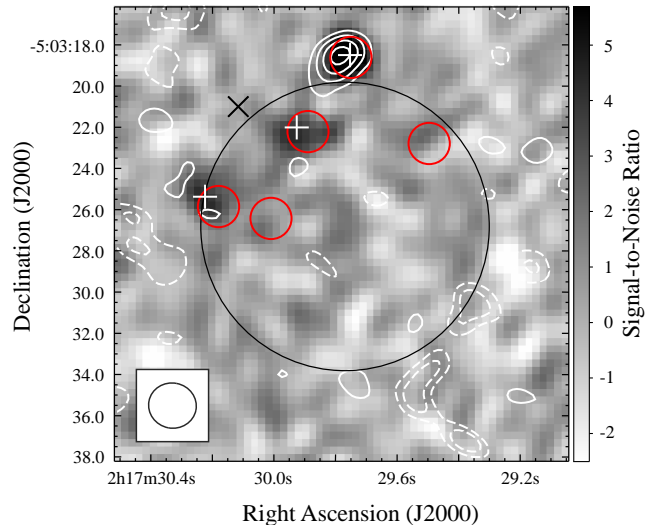


FIG. 1.— The SMA contours overlaid on the VLA 21 cm image. The contours represent -3 , -2 , 2 , 3 , 4 , and 5σ (where $1\sigma = 1.2 \text{ mJy}$). The synthesized beam ($2''.32 \times 2''.19$) is shown in lower left. The dark circle represents the approximate size of the SCUBA/JCMT beam (FWHM $\sim 14''$). The dark cross, white crosses, and red circles are the AzTEC position (Ikarashi et al. in prep.), three radio counterpart candidates in Ivison et al. (2007), and MIPS $24 \mu\text{m}$ sources in the SWIRE catalog, respectively.

is close to zero in declination, the uv coverage is under-sampled in the north-south direction and the resultant synthesized beam has multiple sidelobes at the 30% level along the north-south direction about $14''$ away from the synthesized beam. The final map was made after adding the data from all four days and two sidebands, and corrected for the attenuation by the $35''$ primary beam of the SMA. The astrometric accuracy is likely dominated by the low S/N of the image, and we assess $\sim 0''.4$.

3. RESULTS

The synthesized map is shown in Figure 1. A source was detected at about 6 sigma significance $8''.2$ north of the SCUBA coordinates. The source appears slightly elongated in the northeast-southwest direction but this is likely caused by the low S/N, and the source is entirely unresolved with the SMA beam. Based on a point source fit to the visibilities, the derived flux is $6.9 \pm 1.2 \text{ mJy}$, and the coordinates are $\alpha(\text{J2000}) = 02^{\text{h}} 17^{\text{m}} 29.79^{\text{s}}$ and $\delta(\text{J2000}) = -05^{\circ} 03' 18''.65$. The derived flux is consistent with the SCUBA $850 \mu\text{m}$ flux of $8.15 \pm 2.2 \text{ mJy}$ (Coppin et al. 2006) within the uncertainties of both measurements.

4. MULTI-WAVELENGTH DATA

Multi-wavelength images around SXDF 850.6 are shown in Figure 2. While an obvious optical counterpart is not seen in the images from u to z' bands, the NIR images represented in JHK and longer wavelength images show a presence of a counterpart. The photometry of the counterpart and upper limits at the SMA position are presented in Table 1.

4.1. Radio and Millimeter

Ivison et al. (2007) identify three radio counterpart candidates for SXDF 850.6 in their deep VLA 21 cm

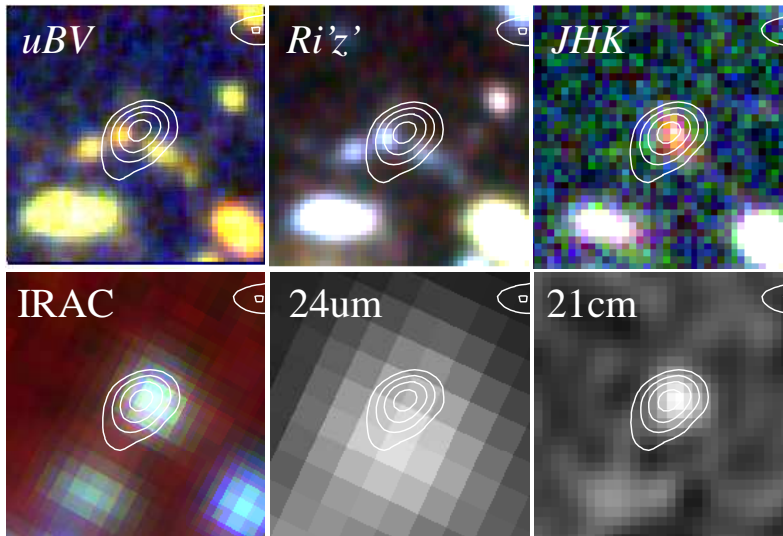


FIG. 2.— Multi-wavelength images of SXDF 850.6 with the SMA contours (2, 3, 4, and 5σ). The size of each image is $10'' \times 10''$ and north is up. From left to right: rgb image of MOSAIC II/*u*, SuprimeCam/*B*, and *V*; rgb image of SuprimeCam/*R*, *i'*, and *z'*; rgb image of WFCAM/*J*, *H*, and *K*; rgb image of IRAC/*ch1* (blue), *ch2* (green), *ch3* and *4* (red); MIPS 24 μm ; VLA 21 cm.

map based on the probability analysis method of Downes et al. (1986). All three radio sources have corresponding MIPS 24 μm sources (Clements et al. 2008), as shown in Figure 1. The SMA observation reveals that the correct radio counterpart is the most distant source from the SCUBA centroid, and the brightest in 24 μm emission. This demonstrates the effectiveness of the SMA in identifying SMG counterparts, especially in situations with multiple counterpart candidates.

The radio coordinates derived from reanalysis of the VLA image (Arumugam et al. in prep.) are α (J2000) = $02^{\text{h}} 17^{\text{m}} 29.755^{\text{s}}$ ($\pm 0.005^{\text{s}}$) and δ (J2000) = $-05^{\circ} 03' 18''.40$ ($\pm 0''.08$), with peak and integrated flux of $99.8 \mu\text{Jy}$ and $100.0 \pm 10.6 \mu\text{Jy}$ respectively. The close similarity of the peak and integrated flux suggests that the radio emission is unresolved with the $1''.79 \times 1''.51$ beam (P.A. = 6.1°).

SXDF 850.6 is detected at 1100 μm with deboosted flux of $3.9 \pm 0.5 \text{ mJy}$ (Ikarashi et al. in prep.) using the AzTEC camera (Wilson et al. 2008) on the Atacama Submillimeter Telescope Experiment (ASTE; Ezawa et al. 2004, 2008). The AzTEC coordinates are consistent with the SMA position within a 2σ error circle.

4.2. Mid-IR

Spitzer/IRAC and MIPS data are taken from the SpUDS archive. The 3σ detection limits are 0.58, 0.89, 5.7, and 5.3 μJy in IRAC bands (3.6, 4.5, 5.8, and 8.0 μm), and 36 μJy in MIPS 24 μm band. The photometry was performed using the SExtractor package (Bertin & Arnouts 1996). The photometry in IRAC bands is conducted with $3''.8$ diameter aperture, and the photometric zero-points of the images are determined using colors of early-type stars between *K*-band and IRAC bands following Lacy et al. (2005). In order to derive total flux, the aperture photometry are corrected by assuming IRAC PSFs by a factor of 1.36, 1.40, 1.65, and 1.84, respectively. The photometry in the 24 μm band is conducted using $12''$ diameter aperture. The aperture

magnitude is corrected by a factor of 1.70.

We find emission at the SMA position in all IRAC bands and MIPS 24 μm band. Note that the 24 μm flux in Table 1 should be used as an upper limit since sources around the SMA position are blended in the 24 μm image (Figure 2).

4.3. JHK

J, *H*, and *K* band images are obtained from UKIDSS (UKIRT InfraRed Deep Sky Surveys) Ultra Deep Survey Third Data Release (Laurent et al. 2005). The 3σ detection limits are 24.28, 24.08, and 24.18 mag, respectively.

A faint source is detected at the SMA position in all bands. We perform photometry using the SExtractor. Aperture photometry with $1''.8$ diameter aperture in the *J*, *H*, and *K* bands are corrected by difference between the aperture and the total (MAG_AUTO) magnitudes in the *K*-band.

4.4. uBVRi'z'

We present a *u*-band image of MOSAIC II on CTIO 4-m telescope (Fujishiro et al. in prep.), *B*, *V*, *R*, *i'*, and *z'* images of SuprimeCam on Subaru telescope in Figure 2. *B*, *V*, *R*, *i'*, and *z'* band images are obtained from Subaru/XMM-Newton Deep Survey database (SXDS; Furusawa et al. 2008). No galaxy is detected at the SMA position in these bands. The 3σ detection limits are 26.00, 27.94, 27.68, 27.43, 27.45, and 26.43 mag, respectively.

Near the SMA position, three galaxies are seen; $\sim 2''$ south-east, $\sim 0''.8$ south-east, and $\sim 1''$ south-west to the SMA position. We derive photometric redshifts for the sources and find that they are likely to be at $z < 1$, and it is unlikely that they are related to the SMA source (see § 5).

5. SED FITTING

We perform SED model fitting to the photometry data from UV to radio to estimate photometric redshifts and

TABLE 1. FLUXES OF SXDF 850.6

Band	Flux	Instrument	Ref.
<i>u</i>	<0.0148 μ Jy	MOSAIC II	1
<i>B</i>	<0.0248 μ Jy	SuprimeCam	1
<i>V</i>	<0.0315 μ Jy	SuprimeCam	1
<i>R</i>	<0.0397 μ Jy	SuprimeCam	1
<i>i'</i>	<0.0389 μ Jy	SuprimeCam	1
<i>z'</i>	<0.0996 μ Jy	SuprimeCam	1
<i>J</i>	$1.40^{+0.23}_{-0.20}$ μ Jy	WFCAM	1
<i>H</i>	$3.21^{+0.23}_{-0.22}$ μ Jy	WFCAM	1
<i>K</i>	9.17 ± 0.23 μ Jy	WFCAM	1
3.6 μ m	29.0 ± 0.8 μ Jy	IRAC	1
4.5 μ m	39.3 ± 1.1 μ Jy	IRAC	1
5.8 μ m	54.3 ± 1.9 μ Jy	IRAC	1
8.0 μ m	38.2 ± 1.4 μ Jy	IRAC	1
24 μ m	630 ± 30 μ Jy	MIPS	1
70 μ m	<30 mJy	MIPS	2
160 μ m	<200 mJy	MIPS	2
450 μ m	<81 mJy	SCUBA	3
850 μ m	8.15 ± 2.2 mJy	SCUBA	3
880 μ m	6.9 ± 1.2 mJy	SMA	1
1100 μ m	3.9 ± 0.5 mJy	AzTEC	4
21 cm	100.0 ± 10.6 μ Jy	VLA	5
0.2–12 keV	$<6.3 \times 10^{-15}$ erg cm $^{-2}$ s $^{-1}$	XMM-Newton	6

REFERENCES. — (1) This work; (2) Flux limits in the SWIRE catalog (Surace et al. in prep.); (3) Coppin et al. 2006; (4) Ikarashi et al. in prep.; (5) Arumugam et al. in prep. (6) FLIX: upper limit server for XMM-Newton data provided by the XMM-Newton Survey Science Centre

NOTE. — Limits are 3σ .

other physical properties (stellar mass, *V*-band extinction, star formation timescale, and metallicity). The photometric data are divided into two wavelength ranges: (1) from UV to 8.0 μ m, where stellar emission is dominant, (2) from submm to radio, where thermal dust and synchrotron emission is dominant.

5.1. UV – Optical – IR

SED fits are performed to the photometry ranging from UV to 8.0 μ m (*u*, *B*, *V*, *R*, *i'*, *z'*, *J*, *H*, *K*, 3.6 μ m, 4.5 μ m, 5.8 μ m, and 8.0 μ m) using the Hyperz code (Bolzonella et al. 2000). We use a synthetic spectral library of GALAXEV (Bruzual & Charlot 2003) for SED templates. We adopt the Calzetti extinction law (Calzetti et al. 2000) and the Chabrier (2003) initial mass function with lower and upper cutoff mass of 0.1 and 100 M_{\odot} . Two star formation histories are assumed: (i) exponentially decaying SFR with a timescale of τ (i.e., $\text{SFR} \propto e^{-t/\tau}$), (ii) constant SFR. We calculate χ^2 values for each SED template with free parameters of redshift ($z = 0\text{--}6$), stellar mass (M_{\star}), *V*-band attenuation ($A_V = 0.0\text{--}6.0$), star formation timescale ($\tau = 0.01\text{--}5$ Gyr), and metallicity ($Z = 1.0, 0.4, 0.2 Z_{\odot}$). The best-fit results are obtained with the exponentially decaying SFR, $z = 1.87^{+0.15}_{-0.07}$, $M_{\star} = 2.5^{+2.2}_{-0.3} \times 10^{11} M_{\odot}$, $A_V = 3.0^{+0.3}_{-1.0}$ mag, and age = 720^{+1880}_{-210} Myr (Table 2 and Figure 3). The results suggest that SXDF 850.6 has a large population of old stars, with large amount of dust obscuring the stellar emission. The stellar mass is comparable to those of massive star-forming galaxies at $z \sim 2$ (e.g., Shapley et al. 2005; Erb et al. 2006a) and consistent with stellar masses recently derived for other SMGs ($\sim 10^{11}\text{--}10^{12} M_{\odot}$) (e.g., Dye et al. 2008;

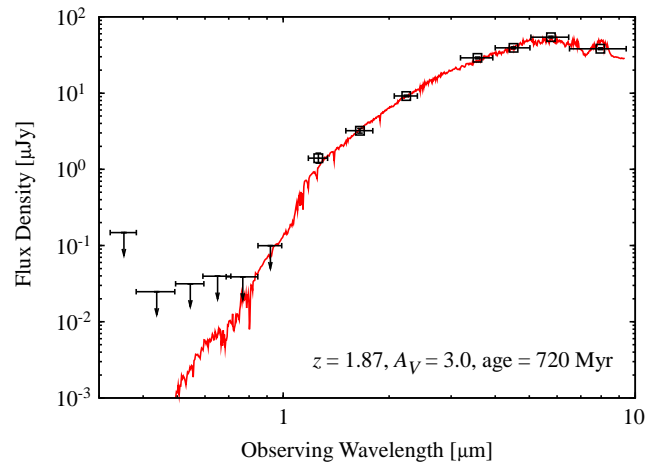


FIG. 3.— Best-fit SED obtained in UV–optical–IR SED fit along with photometry data. Downward arrows represent 3σ upper limits.

Michałowski et al. 2009).

5.2. Submm – Radio

Photometry at 850 μ m, 880 μ m, 1100 μ m, and 21 cm is used for submm-radio SED fits. The MIPS photometry is also used to check for consistency. We use the following starburst SED models: Arp 220 (Silva et al. 1998), the average SED of 76 SMGs with spectroscopic redshifts (Michałowski et al. 2009), and 105 SED models of Chary & Elbaz (2001). We perform minimized χ^2 fits with free parameters of redshifts and flux scaling factors. We find the best-fit redshifts of $z = 2.1^{+0.5}_{-0.4}$ for Arp 220 ($\chi^2 = 0.3$), $z = 1.8^{+0.5}_{-0.3}$ for the average SMG ($\chi^2 = 0.4$), and $z = 2.5^{+0.6}_{-0.4}$ for an SED of Chary & Elbaz (2001) ($\chi^2 = 0.09$). The errors are 99% confidence intervals. Note that there are other templates in the library of Chary & Elbaz (2001) that fit the photometry data with similar χ^2 values in the redshift range of $z \sim 1\text{--}3$. The derived redshifts are consistent with the result in the UV-optical-IR SED fit in the previous section. The IR luminosities are estimated to be $L_{\text{IR}} = (7\text{--}26) \times 10^{12} L_{\odot}$ from the intrinsic IR luminosities of SED templates multiplied by scaling factors for the best-fit SEDs. The best-fit SED models are shown in Figure 4 with photometry data from UV to radio. All of the SEDs overestimate the UV–NIR photometry, suggesting that stellar emission is heavily attenuated by dust. This is consistent with the large extinction ($A_V = 3.0$) derived from the UV–optical–IR SED fit. Finally, we note that the SMG sample in Michałowski et al. (2009) is biased against optically faint objects. It is clearly important to take into account a heavily obscured SMG like SXDF 850.6 (or e.g., GOODS 850-5 in Wang et al. 2009, AzTEC1 in Tamura et al. in prep.) to properly understand the overall picture of SMGs.

6. DISCUSSION

6.1. AGN Contribution

The rest-frame 1.6 μ m bump is clearly seen at 5.8 μ m (Figure 3), suggesting that the NIR emission detected in the IRAC bands is star-formation dominated (e.g., Weedman et al. 2006; Farrah et al. 2008). The flatter

TABLE 2. BEST-FIT RESULTS IN UV–OPTICAL–IR SED FIT

z	M_\star (M_\odot)	A_V (mag)	Age (Myr)	τ (Myr)	Z (Z_\odot)	χ^2
(1)	(2)	(3)	(4)	(5)	(6)	(7)
$1.87^{+0.15}_{-0.07}$	$2.5^{+2.2}_{-0.3} \times 10^{11}$	$3.0^{+0.3}_{-1.0}$	720^{+1880}_{-210}	20	1	13.4

NOTE. — The errors are 68% confidence intervals. (1) photometric redshift; (2) stellar mass; (3) V -band attenuation; (4) age; (5) star formation timescale; (6) metallicity; (7) χ^2 value

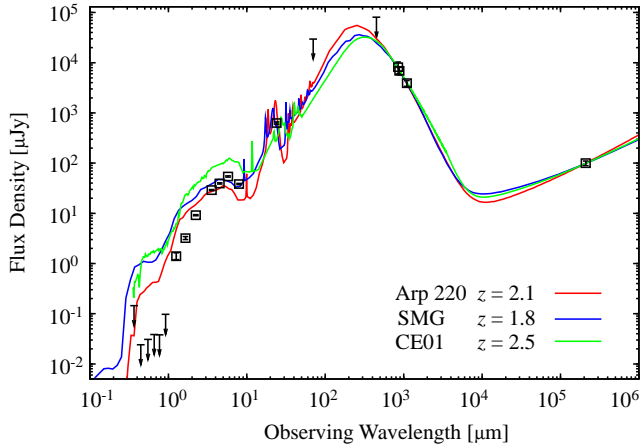


FIG. 4.— Best-fit SEDs for three different models obtained in submm–radio SED fit. The SEDs are the average SED of 76 SMGs (Michałowski et al. 2009) at $z = 1.8$, Arp 220 (Silva et al. 1998) at $z = 2.1$, and a starburst template of Chary & Elbaz (2001) at $z = 2.5$. Photometry data from UV to radio are overplotted.

spectral slope in the IRAC emission compared to AGN populations favours a star formation as a dominant heating source (Yun et al. 2008; Ivison et al. 2004). This is also supported by the fact that SXDF 850.6 appears close to the starburst model tracks in the $S_{8.0}/S_{4.5}$ vs. $S_{24}/S_{8.0}$ color-color diagram of Ivison et al. (2004). These facts suggest that SXDF 850.6 favours star formation as a dominant heating source and the physical quantities derived in the SED fit are less affected by the AGN.

The 3σ upper limit on the rest-frame X-ray luminosity derived from 0.2–12 keV flux is 1.3×10^{44} erg s^{-1} (assuming $z = 1.87$ and an effective photon index of $\Gamma = 1.8$). Since this value is not properly corrected for hydrogen attenuation, we do not constrain the AGN contribution from the X-ray luminosity.

6.2. Dust Mass and Molecular Gas Mass

Assuming the observed 880 μm flux is dominated by thermal dust emission, the dust mass can be derived as $M_d = S_{\text{obs}} D_L^2 / [(1+z)\kappa_d(\nu_{\text{rest}})B(\nu_{\text{rest}}, T_d)]$ (e.g., Hughes et al. 1997), where S_{obs} is the observed flux density, ν_{rest} is the rest-frame frequency, $\kappa_d(\nu_{\text{rest}})$ is the dust mass absorption coefficient, T_d is the dust temperature, and $B(\nu_{\text{rest}}, T_d)$ is the Planck blackbody function. We assume that the absorption coefficient varies as $\kappa_d \propto \nu^\beta$ and β lies between 1 and 2 (e.g., Hildebrand 1983). We adopt $\kappa_d(125 \mu\text{m}) = 2.64 \pm 0.29$ $\text{m}^2 \text{kg}^{-1}$, the average value of various studies (Dunne et al. 2003), $T_d = 30\text{--}50$ K, and $\beta = 1.5$, the typical values for SMGs

(e.g., Kovács et al. 2006; Pope et al. 2006; Coppin et al. 2008; Michałowski et al. 2009). The dust mass is estimated to be $M_d = (4\text{--}9) \times 10^8 M_\odot$ for SXDF 850.6 at $z = 1.87$. This is consistent with previous work on SMGs (e.g., Kovács et al. 2006; Coppin et al. 2008; Michałowski et al. 2009).

By adopting a gas-to-dust mass ratio of 54, which is an average value for SMGs in Kovács et al. (2006), the molecular gas mass is $M_{\text{gas}} = (2\text{--}5) \times 10^{10} M_\odot$.

6.3. Star Formation Activity and Nature of SXDF 850.6

The UV–IR SED exhibits quiescent star forming activity dominated by old stellar components. The current SFR estimated from the SED fit is approximately zero. This is because the large part of the stellar mass was formed at the early phase of star formation and SFR decreased with time following exponential decay ($\tau = 20$ Myr for the best-fit SED). On the other hand, the IR luminosity of the best-fit submm–radio SED provides $\text{SFR}_{\text{IR}} = 1300\text{--}4500 M_\odot \text{yr}^{-1}$ (Kennicutt 1998). The SFR derived from 1.4 GHz radio emission is $1400 M_\odot \text{yr}^{-1}$ following the equation of Bell (2003), and $1100 M_\odot \text{yr}^{-1}$ following Yun & Carilli (2002) (with a spectral index of -0.8 and a radio–FIR normalization factor of 1).

To see whether the observational data allow the coexistence of the old stellar SED with quiescent star formation and the dusty starburst SED, we create synthetic SEDs at UV–IR wavelength using the GALAXEV library. The synthetic SEDs are composites of an SED with the same parameters as the best-fit SED which is dominated by old stellar population and starburst SEDs with different parameters. We find that the composite SEDs with plausible parameters for starburst SEDs (e.g., $\text{SFR} \sim 2000 M_\odot \text{yr}^{-1}$, $A_V = 3.0$, and age = 1 Myr) are consistent with the photometry data (Figure 5). Note that combining the SEDs increases the total stellar mass by only $\sim 1\%$.

Combining these results allows us to infer the nature of SXDF 850.6: it is a mature system with a large fraction of old stellar components, and currently experiencing a vigorous dusty starburst. The coexistence of old stars and a current starburst in an SMG is suggested by Wang et al. (2009) from a detailed SED analysis. SXDF 850.6 has enough molecular gas mass as estimated in § 6.2 to maintain intense star formation. Such significant star formation is likely caused by major mergers (e.g., Greve et al. 2005; Tacconi et al. 2006, 2008; Narayanan et al. 2009). If the star formation continues with $\text{SFR} \sim$ a few $10^3 M_\odot \text{yr}^{-1}$, the gas consumption time is \sim a few 10 Myr. This scenario is well described by hydrodynamic simulations of Narayanan et al. (2009) in which a major merger with a $\sim 10^{13} M_\odot$ dark matter

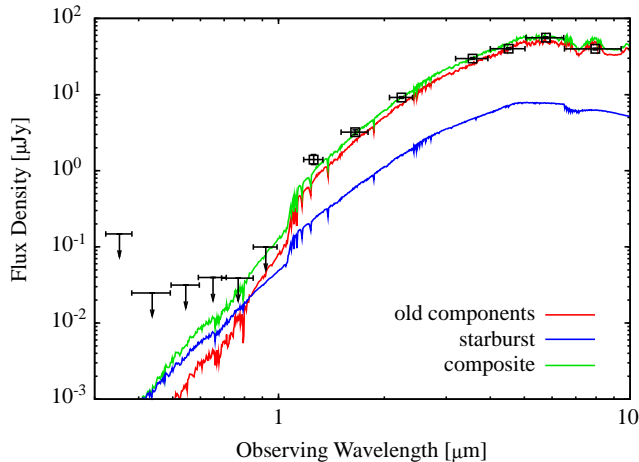


FIG. 5.— Synthetic SEDs of old stellar components (red), starburst components at the age of 100 Myr with an initial SFR of $3000 M_{\odot} \text{ yr}^{-1}$ (blue), and a sum of both (green) created with the GALAXEV library. Photometry data are also shown.

halo produces a peak flux of $\sim 7\text{--}8$ mJy at $850 \mu\text{m}$ for a short duration (< 50 Myr). We are observing the short-lived glow of SXDF 850.6 as a bright SMG. Even if all the molecular gas converts into stars, the total stellar mass will increase by at most 30%. This supports an idea that the large fraction of stellar mass in SMGs is constructed before the current submm bright phase (e.g., Borys et al. 2005; Dye et al. 2008; Michałowski et al. 2009).

The specific star formation rate (SSFR; SFR per unit stellar mass, an estimator of current star-forming activity) of $\sim 5\text{--}20 \text{ Gyr}^{-1}$ places SXDF 850.6 on the high mass end of the correlation between stellar mass and SFR for $z \sim 2$ star-forming galaxies or above the correlation (e.g., Erb et al. 2006b; Reddy et al. 2006; Daddi et al. 2007). If the large population of stars were constructed before the current starburst phase, the enhancement of star formation could be due to merging of massive star forming galaxies (e.g., merging BzKs; Takagi et al. 2008),

and it is possible that this galaxy evolves into a massive present-day elliptical through major merger events (e.g., Lilly et al. 1999; Smail et al. 2004).

7. SUMMARY

We conducted SMA $880 \mu\text{m}$ observations of a submillimeter galaxy, SXDF 850.6, detected with SCUBA in the Subaru/*XMM-Newton* Deep Field, which has multiple radio and IR counterpart candidates. The precise astrometry with the SMA shows that the correct counterpart is the most distant radio source from the SCUBA coordinates. Although there is a lack of a corresponding source at the SMA position in deep images of u , B , V , R , i' , z' bands, we find a counterpart at J , H , K , $3.6 \mu\text{m}$, $4.5 \mu\text{m}$, $5.8 \mu\text{m}$, $8.0 \mu\text{m}$, $24 \mu\text{m}$, $1100 \mu\text{m}$, and 21 cm . A detailed analysis of fitting a library of synthetic SEDs to the photometry from the u -band to $8.0 \mu\text{m}$ gives the best-fit parameters of $z = 1.87_{-0.07}^{+0.15}$, $M_{\star} = 2.5_{-0.3}^{+2.2} \times 10^{11} M_{\odot}$, $A_V = 3.0_{-1.0}^{+0.3} \text{ mag}$, and age = $720_{-210}^{+1880} \text{ Myr}$. The SED fit to the submm–radio photometry using the three different starburst SED models provides the consistent redshift of $z \sim 1.8\text{--}2.5$ and $L_{\text{IR}} = (7\text{--}26) \times 10^{12} L_{\odot}$. The IR color diagnostic suggests that the AGN contribution to the SED is small. The SFR derived from the IR luminosity is $1300\text{--}4500 M_{\odot} \text{ yr}^{-1}$, and the SSFR is $\sim 10 \text{ Gyr}^{-1}$. If the intense starburst continues, the estimated molecular gas mass of $(2\text{--}5) \times 10^{10} M_{\odot}$ will last for a few Myr. Given these facts, it is suggested that SXDF 850.6 is a mature system that already contains a dominant fraction of its expected final stellar mass in an old stellar population, and which is also experiencing a significant starburst. The enhancement of star formation could be due to major mergers.

We thank the anonymous referee for valuable comments. B. H. is financially supported by a Research Fellowship from the JSPS for Young Scientists. JSD acknowledges the support of the Royal Society through a Wolfson Research Merit award.

REFERENCES

- Alexander, D. M., Bauer, F. E., Chapman, S. C., Smail, I., Blain, A. W., Brandt, W. N., & Ivison, R. J. 2005, *ApJ*, 632, 736
Austermann, J. E., et al. 2009, *MNRAS*, 393, 1573
Barger, A. J., Cowie, L. L., & Richards, E. A. 2000, *AJ*, 119, 2092
Barger, A. J., Cowie, L. L., Sanders, D. B., Fulton, E., Taniguchi, Y., Sato, Y., Kawara, K., & Okuda, H. 1998, *Nature*, 394, 248
Bell, E. F. 2003, *ApJ*, 586, 794
Bertin, E., & Arnouts, S. 1996, *A&AS*, 117, 393
Blain, A. W., Smail, I., Ivison, R. J., Kneib, J.-P., & Frayer, D. T. 2002, *Phys. Rep.*, 369
Bolzonella, M., Miralles, J.-M., & Pelló, R. 2000, *A&A*, 363, 476
Borys, C., Smail, I., Chapman, S. C., Blain, A. W., Alexander, D. M., & Ivison, R. J. 2005, *ApJ*, 635, 853
Bruzual, G., & Charlot, S. 2003, *MNRAS*, 344, 1000
Calzetti, D., Armus, L., Bohlin, R. C., Kinney, A. L., Koornneef, J., & Storchi-Bergmann, T. 2000, *ApJ*, 533, 682
Capak, P., et al. 2008, *ApJ*, 681, L53
Chabrier, G. 2003, *ApJ*, 586, L133
Chapman, S. C., Blain, A. W., Smail, I., & Ivison, R. J. 2005, *ApJ*, 622, 772
Chary, R., & Elbaz, D. 2001, *ApJ*, 556, 562
Clements, D. L., et al. 2008, *MNRAS*, 387, 247
Coppin, K., et al. 2006, *MNRAS*, 372, 1621
Coppin, K., et al. 2008, *MNRAS*, 384, 1597
Coppin, K., et al. 2009, arXiv:0902.4464
Daddi, E., et al. 2007, *ApJ*, 670, 156
Daddi, E., et al. 2009, *ApJ*, 694, 1517
Downes, A. J. B., Peacock, J. A., Savage, A., & Carrie, D. R. 1986, *MNRAS*, 218, 31
Dunne, L., Eales, S. A., & Edmunds, M. G. 2003, *MNRAS*, 341, 589
Dye, S., et al. 2008, *MNRAS*, 386, 1107
Erb, D. K., Steidel, C. C., Shapley, A. E., Pettini, M., Reddy, N. A., & Adelberger, K. L. 2006, *ApJ*, 646, 107
Erb, D. K., Steidel, C. C., Shapley, A. E., Pettini, M., Reddy, N. A., & Adelberger, K. L. 2006, *ApJ*, 647, 128
Ezawa, H., et al. 2008, *Proc. SPIE*, 7012
Ezawa, H., Kawabe, R., Kohno, K., & Yamamoto, S. 2004, *Proc. SPIE*, 5489, 763
Farrah, D., et al. 2008, *ApJ*, 677, 957
Furusawa, H., et al. 2008, *ApJS*, 176, 1
Greve, T. R., et al. 2005, *MNRAS*, 359, 1165
Greve, T. R., Ivison, R. J., Bertoldi, F., Stevens, J. A., Dunlop, J. S., Lutz, D., & Carilli, C. L. 2004, *MNRAS*, 354, 779
Hildebrand, R. H. 1983, *QJRAS*, 24, 267
Ho, P. T. P., Moran, J. M., & Lo, K. Y. 2004, *ApJ*, 616, L1
Hughes, D. H., Dunlop, J. S., & Rawlings, S. 1997, *MNRAS*, 289, 766
Hughes, D. H. et al. 1998, *Nature*, 394, 241
Iono, D., et al. 2006, *ApJ*, 640, 1
Iono, D., et al. 2006, *ApJ*, 645, 97
Ivison, R. J., et al. 2002, *MNRAS*, 337, 1

- Iverson, R. J., et al. 2004, *ApJS*, 154, 124
- Iverson, R. J., et al. 2005, *MNRAS*, 364, 1025
- Iverson, R. J., et al. 2007, *MNRAS*, 380, 199
- Iverson, R. J., et al. 2008, *MNRAS*, 390, 1117
- Iverson, R. J., Smail, I., Barger, A. J., Kneib, J.-P., Blain, A. W., Owen, F. N., Kerr, T. H., & Cowie, L. L. 2000, *MNRAS*, 315, 209
- Iverson, R. J., Smail, I., Le Borgne, J.-F., Blain, A. W., Kneib, J.-P., Bezecourt, J., Kerr, T. H., & Davies, J. K. 1998, *MNRAS*, 298, 583
- Kennicutt, R. C., Jr. 1998, *ARA&A*, 36, 189
- Kovács, A., Chapman, S. C., Dowell, C. D., Blain, A. W., Iverson, R. J., Smail, I., & Phillips, T. G. 2006, *ApJ*, 650, 592
- Lacy, M., et al. 2005, *ApJS*, 161, 41
- Lawrence, A., et al. 2007, *MNRAS*, 379, 1599
- Laurent, G. T., et al. 2005, *ApJ*, 623, 742
- Lilly, S. J., Eales, S. A., Gear, W. K. P., Hammer, F., Le Fèvre, O., Crampton, D., Bond, J. R., & Dunne, L. 1999, *ApJ*, 518, 641
- Michalowski, M. J., Hjorth, J., & Watson, D. 2009, arXiv:0905.4499
- Mortier, A. M., et al. 2005, *MNRAS*, 363, 563
- Narayanan, D., Hayward, C. C., Cox, T. J., Hernquist, L., Jonsson, P., Younger, J. D., & Groves, B. 2009, arXiv:0904.0004
- Neri, R., et al. 2003, *ApJ*, 597, L113
- Perera, T. A., et al. 2008, *MNRAS*, 391, 1227
- Pope, A., et al. 2006, *MNRAS*, 370, 1185
- Reddy, N. A., Steidel, C. C., Fadda, D., Yan, L., Pettini, M., Shapley, A. E., Erb, D. K., & Adelberger, K. L. 2006, *ApJ*, 644, 792
- Sault, R. J., Teuben, P. J., & Wright, M. C. H. 1995, *Astronomical Data Analysis Software and Systems IV*, 77, 433
- Scott et al. 2002, *MNRAS*, 331, 817
- Scott, K. S., et al. 2008, *MNRAS*, 385, 2225
- Scoville, N. Z., Carlstrom, J. E., Chandler, C. J., Phillips, J. A., Scott, S. L., Tilanus, R. P. J., & Wang, Z. 1993, *PASP*, 105, 1482
- Shapley, A. E., Steidel, C. C., Erb, D. K., Reddy, N. A., Adelberger, K. L., Pettini, M., Barmby, P., & Huang, J. 2005, *ApJ*, 626, 698
- Silva, L., Granato, G. L., Bressan, A., & Danese, L. 1998, *ApJ*, 509, 103
- Smail, I., Chapman, S. C., Blain, A. W., & Iverson, R. J. 2004, *ApJ*, 616, 71
- Smail, I., Iverson, R. J., Owen, F. N., Blain, A. W., & Kneib, J.-P. 2000, *ApJ*, 528, 612
- Smail, I., Iverson, R. J. & Blain, A. W. 1997, *ApJ*, 490, 5 & Keel, W. C. 2004, *ApJ*, 617, 64
- Tacconi, L. J., et al. 2006, *ApJ*, 640, 228
- Tacconi, L. J., et al. 2008, *ApJ*, 680, 246
- Takagi, T., Ono, Y., Shimasaku, K., & Hanami, H. 2008, *MNRAS*, 389, 775
- Tamura, Y., et al. 2009, *Nature*, 459, 61
- Wagg, J., Owen, F., Bertoldi, F., Sawitzki, M., Carilli, C. L., Menten, K. M., & Voss, H. 2009, *ApJ*, 699, 1843
- Wang, W.-H., Cowie, L. L., van Saders, J., Barger, A. J., & Williams, J. P. 2007, *ApJ*, 670, L89
- Wang, W.-H., Barger, A. J., & Cowie, L. L. 2009, *ApJ*, 690, 319
- Weedman, D., et al. 2006, *ApJ*, 653, 101
- Wilson, G. W., et al. 2008a, *MNRAS*, 386, 807
- Younger, J. D., et al. 2007, *ApJ*, 671, 1531
- Younger, J. D., et al. 2008, *MNRAS*, 387, 707
- Yun, M. S., & Carilli, C. L. 2002, *ApJ*, 568, 88
- Yun, M. S., et al. 2008, *MNRAS*, 389, 333